CHAPTER – 3

Phase Evolution and Thermal Stability of MgAlSiCrFe LDHEA Alloy Processed through Mechanical Alloying and Spark Plasma Sintering

CHAPTER 3

PHASE EVOLUTION AND THERMAL STABILITY OF MgAlSiCrFe LOW-DENSITY HIGH ENTROPY ALLOY PROCESSED THROUGH MECHANICAL ALLOYING AND SPARK PLASMA SINTERING

The present chapter deals with the development of low-density equiatomic MgAlSiCrFe high-entropy alloy (HEA) by incorporating elements like Mg and Si (having HCP and diamond cubic crystal structure respectively) with Al (FCC), Cr (BCC) and Fe (BCC) elements and processing through mechanical alloying. The alloying behavior, phase evolution, phase composition and thermal stability of as-milled nanostructured powders and sintered compacts of HEA were ascertained through X-ray diffraction (XRD), transmission electron microscopy (TEM), scanning electron microscopy (SEM) and differential scanning calorimetry (DSC), respectively. Furthermore, the experimental findings were correlated with various thermodynamic parameters for understanding the phase evolution and stability. Attempts were made to explore the mechanical properties of the alloy through microindentation techniques. The phases evolved during MA and SPS were explained with the help of the thermodynamic parameters and property diagrams generated through the CALPHAD approach using Thermo Calc software.

3.1 Alloying behavior and phase evolution of milled MgAlSiCrFe HEA powder

The schematic diagram for synthesizing MgAlSiCrFe LDHEA is displayed in Figure 3.1 (a). The phase evolution during mechanical alloying of this LDHEA powder is represented in Figure 3.1(b). The XRD patterns corresponding to of 1h, 10h, 40h and 60 h mechanically alloyed powders demonstrate the sequence of phase evolution and dissolution of elements into the solid solution during milling. The XRD pattern for 1 h milled sample shows the intense reflections corresponding to all the alloying elements, i.e. Mg, Al, Si, Cr and Fe.

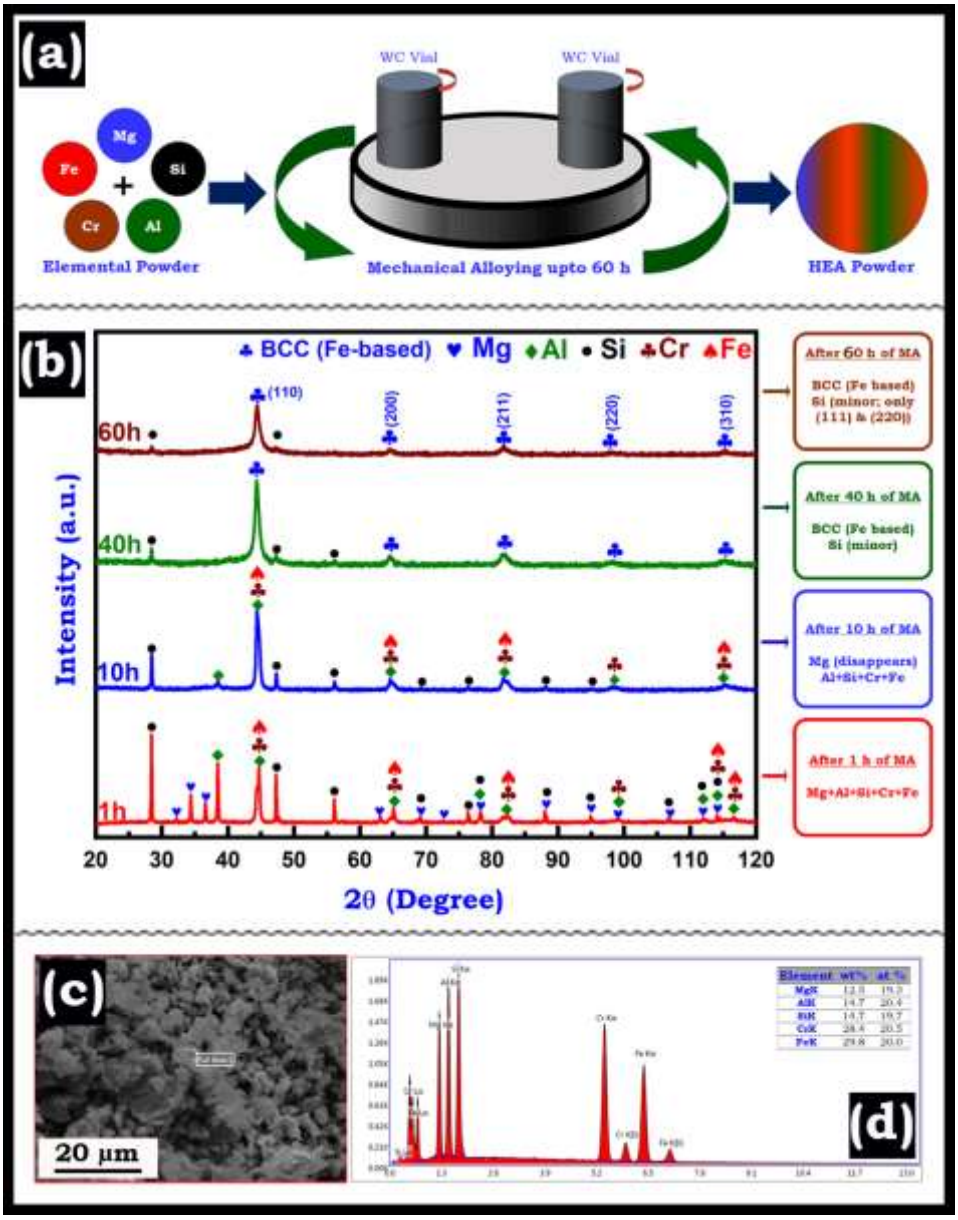

Figure 3.1: Phase evolution after 60 h of mechnical alloying MgAlSiCrFe HEA powder (a); SEM micrograph showing the the morphology of 60 h milled powder scanned for elemental analysis (b); (c) SEM micrograph 60h milled powder; (d) EDS-Spectrum showing the presence of alloying element and elemental composition after 60 h of milling.

After 10 h of milling, all the reflections corresponding to the Mg disappeared along with the minor peaks pertaining to Al. On further milling until 40 h, all the alloying elements dissolved into the solid solution and formed a BCC phase (a=0.2887±0.005 nm). However, along with the BCC phase, a minor amount of Si was found to be undissolved.

Even after continuing the milling till 60 h, ~3% of Si could not be dissolved in the solid solution. The minor fraction of this Si was detected from the most intense reflections i.e. (111) and (220) of the XRD pattern. It may be speculated that at higher milling duration Si can be forced to be dissolved during milling. Figure 3.1 (c) and (d) represent the SEM micrograph and EDS spectrum of the LDHEA powder milled for 60 h. From the EDS spectrum, it is evident that the composition is close to that of the nominal composition. Figure 3.2 (a), (b) and (c) represents the TEM bright field (BF) image, selected area diffraction (SAD) pattern and dark field (DF) image respectively of powder milled for 60 h. The BF image shows the presence of the nanoscrystalline grain along with the secondary particles and dark patches. The dark patches observed in the BF image of Figure 3.2 (a) may be due to the strain accumulation during mechanical alloying. The presence of secondary particle envisaged in BF image has been confirmed with SAD pattern, where the presence of the BCC phase along with the minor amount of undissolved Si was discerned. The polycrystalline rings corresponding to the (110), (200), and (211) reflections of the BCC phase were identified. Along with the BCC phase, a specific spot corresponding to (111) reflection of Si and polycrystalline ring of weak intensity corresponding to the (220) reflection of Si was also detected from the electron diffraction pattern. The SAD pattern shown in Figure 3.2 (b) is in close agreement with that of XRD findings. The DF image of milled powder shows nanostructured grains (≤ 20 nm) and undissolved Si particles distributed in the BCC solid solution matrix. The DF image shown in Figure 3.2 (c) corresponds to the (110) reflection of BCC and (220) polycrystalline ring of Si as marked with the red circle.

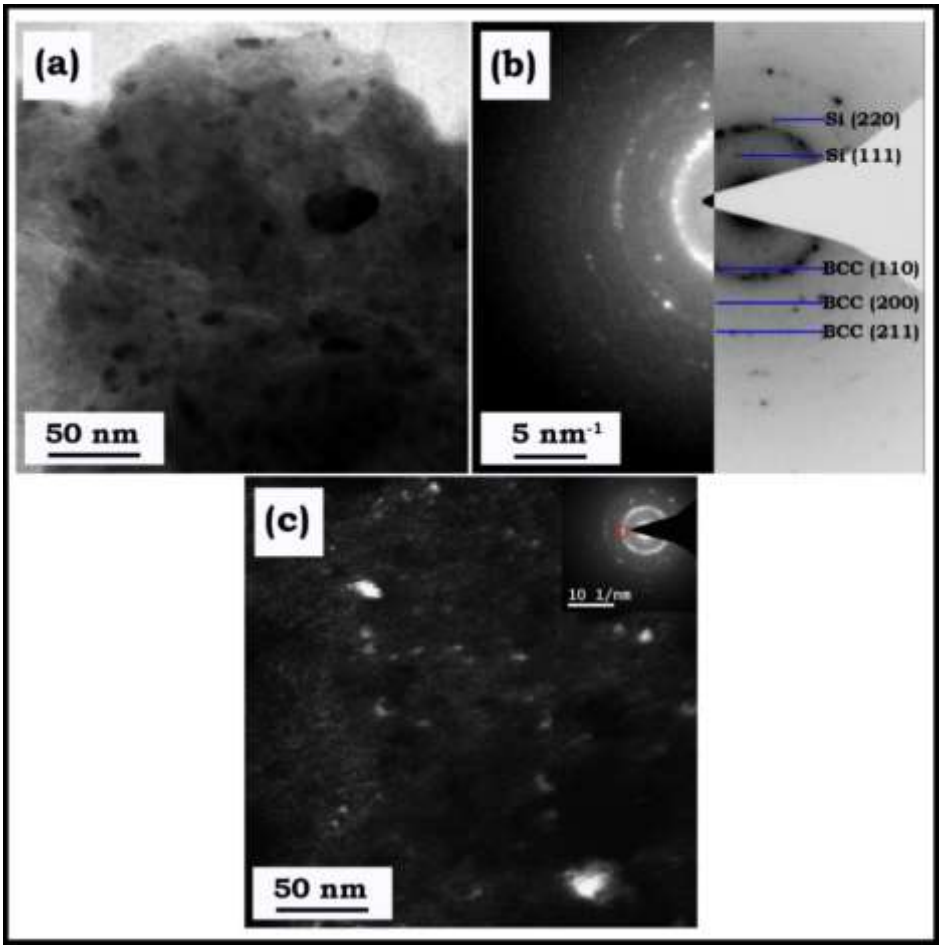

Figure 3.2: TEM micrograph showing (a) bright-field image; (b) corresponding SAD pattern; (c) dark-field image of MgAlSiCrFe HEA powder milled for 60 h.

The STEM-EDS mapping of mechanically alloyed LDHEA powder particles was carried out to establish the elemental distribution (Figure 3.3). The STEM-EDS mapping shown in Figure 3.3 (a) represents the homogenous distribution of intensity of elements corresponding to Mg, Al, Si, Cr, and Fe in the milled powder. The minor variation in intensity from Cr and Fe in the particle may be corroborated with the variation in the thickness and morphology of milled powder. The STEM-EDS mapping technique is essentially a mass-thickness contrast imaging. Therefore, the x-ray signals generated

during mapping are also influenced by the morphology and thickness of the powder particle being investigated.

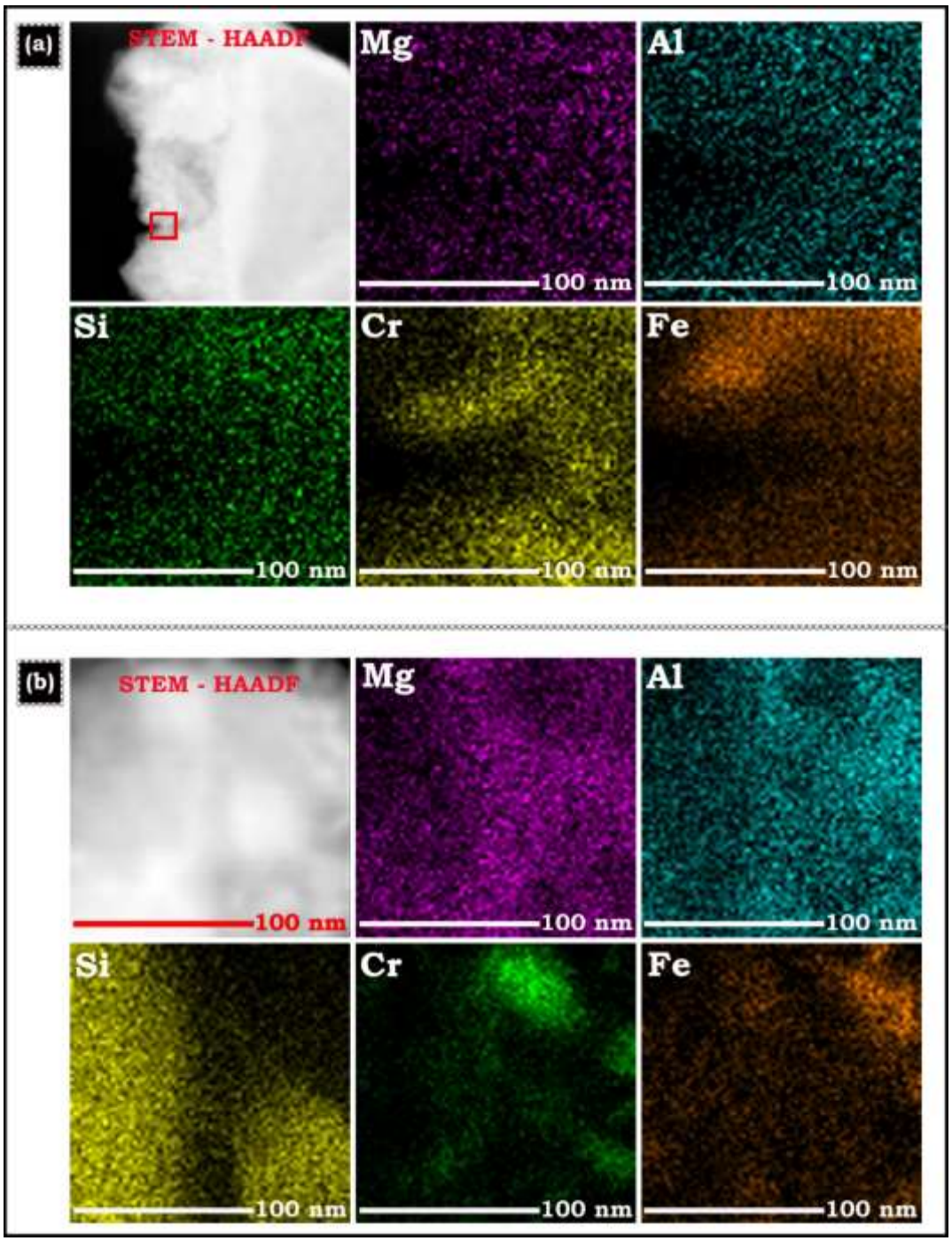

Figure 3.3: STEM – EDS mapping of equiatomic MgAlSiCrFe LDHEA powder milled for 60 h (a) showing homogenous elemental distribution; (b) showing presence of homogenous elemental distribution of apart from Si (depicting the presence of minor fraction of retained Si).

These variations of the parameters influence the x-ray signals generated after interaction with the milled particles. However, the same condition does not prevail for the milled particle as shown in Figure 3.3 (b), which shows that the elements like Mg and Al are almost homogeneously distributed. The particle having a Si-rich region can be observed as evident from its intensity.

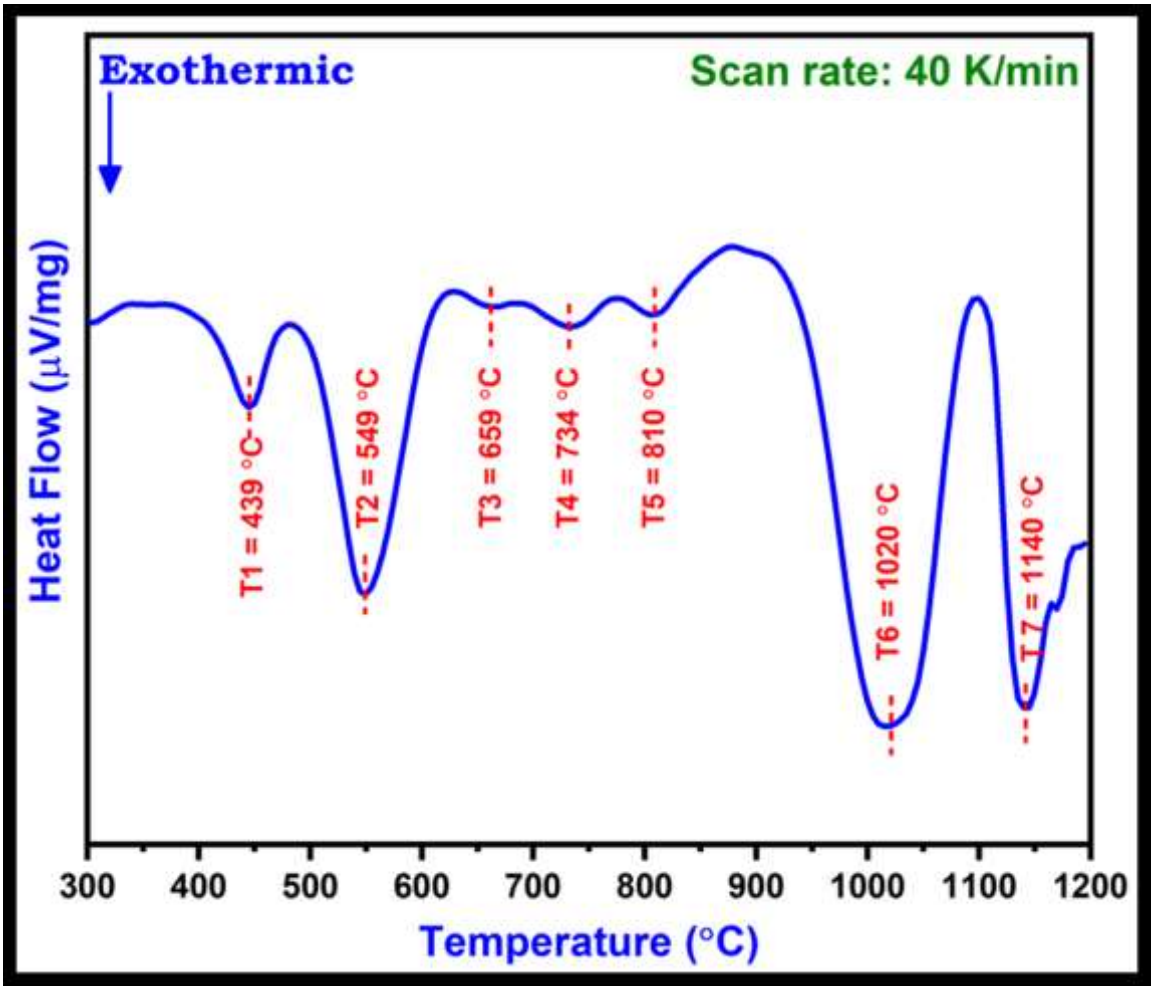

Figure 3.4: DSC thermogram of MgAlSiCrFe high entropy alloy powder milled for 60 h upto 1200 ℃ (1473 K).

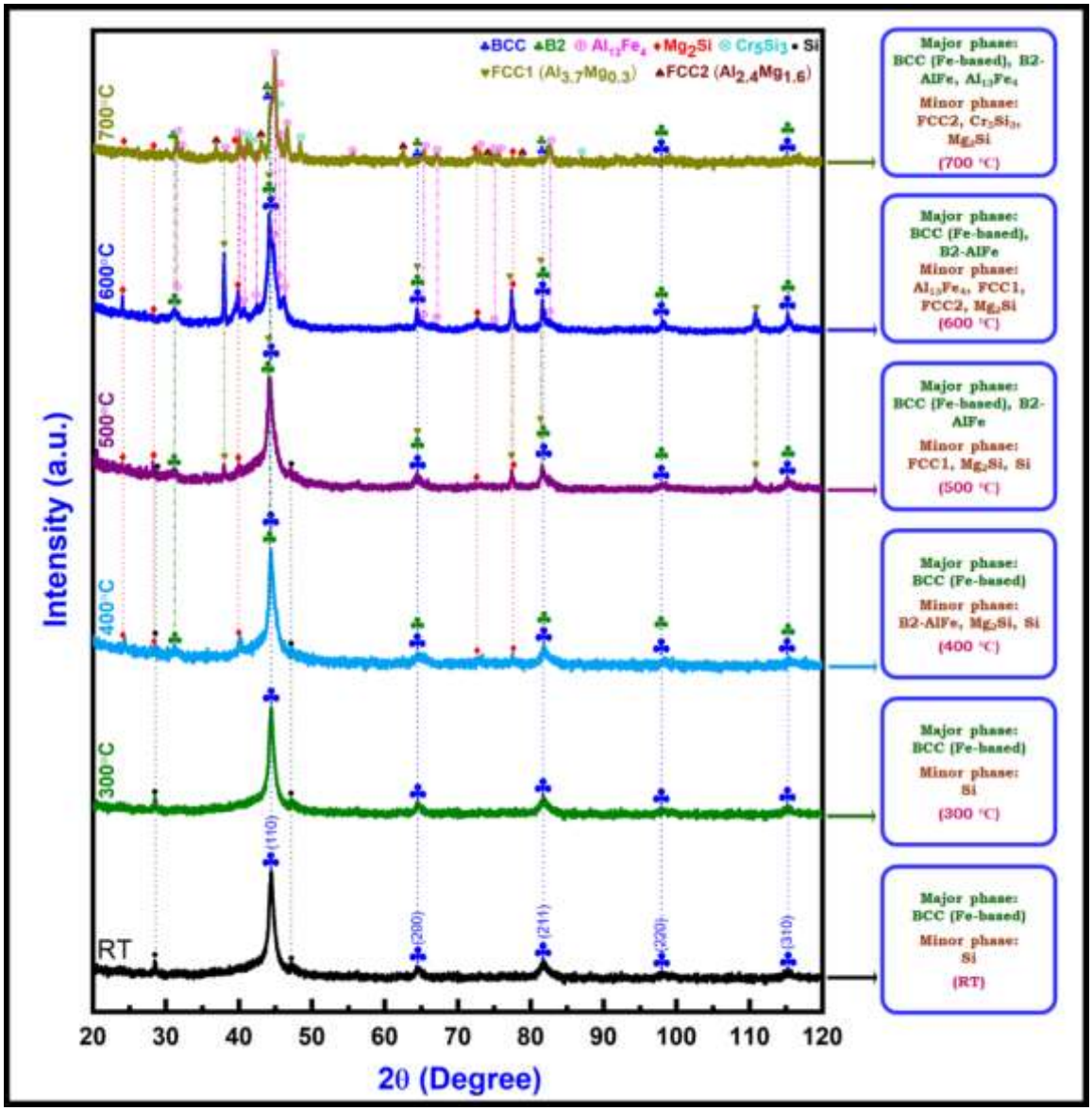

Figure 3.5: Sequence of phase evolution during isothermal heating from room temperature to 700 ℃ (973 K) for 60 h milled MgAlSiCrFe HEA.

The region rich in Si are found to be lean in Cr and Fe and have an almost uniform distribution of Mg and Al. The area having the uniform composition of Mg, Al, Cr, and Fe are lean in Si, which are discerned from its intensity. The homogenous distribution of elements like Mg and Al may be attributed to its low melting point and high self-diffusion co-efficient (as mentioned in the **Table 3.3**). The STEM-EDS results are in good agreement with the findings observed through the XRD pattern and TEM results.

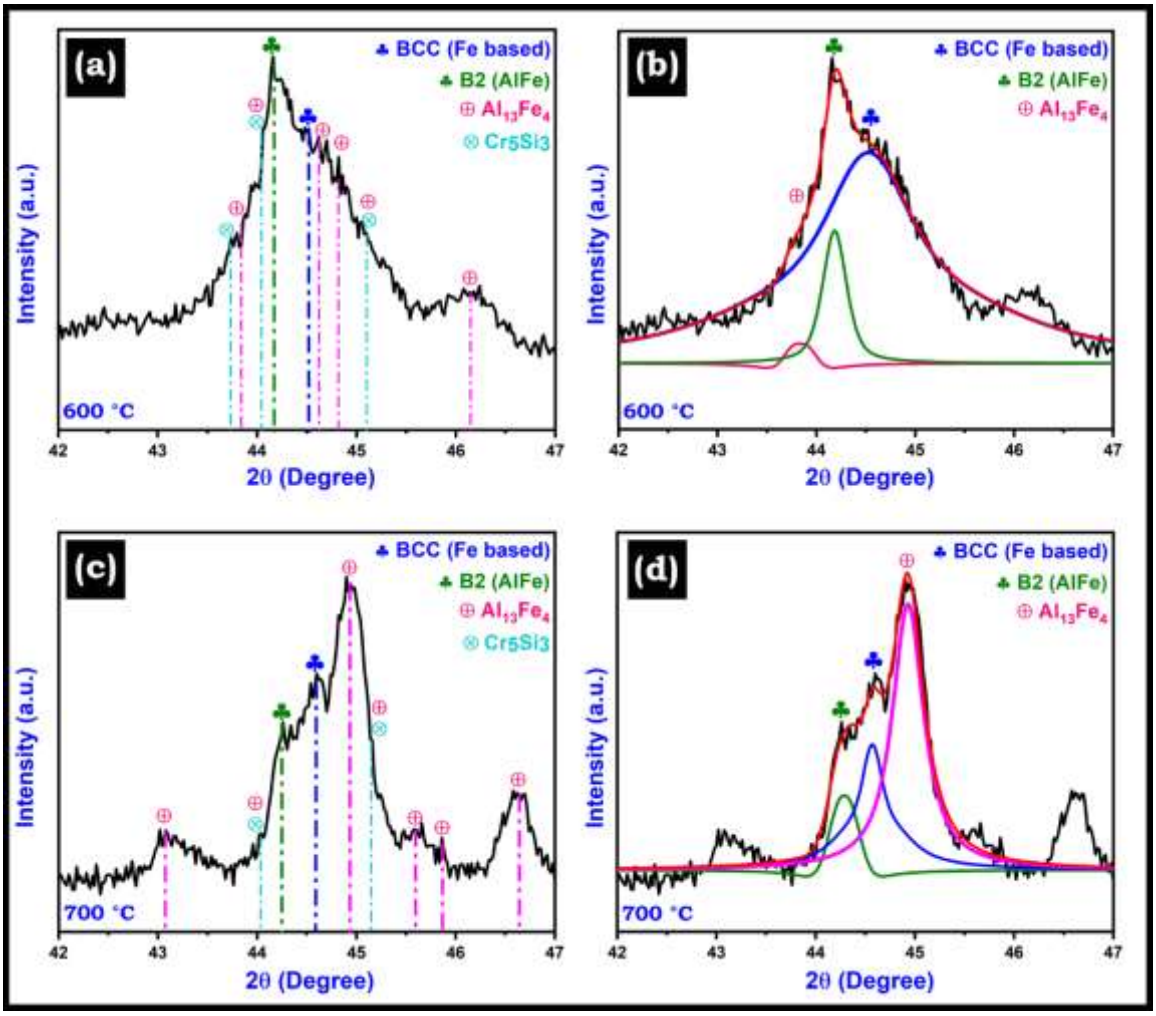

Figure 3.6: Exploded XRD plot showing the evolution of phases along with (110) reflection of BCC (Fe-based) and B2 (AlFe) type phase at (a) 600 ℃ (873 K) and (c) 700 ℃ (973 K) respectively. Deconvolution of peaks showing presence of BCC (Fe-based), B2 (AlFe) and $Al_{13}Fe_4$ phase at (b) 600 ℃ (873 K) and (d) 700 ℃ (973 K) respectively.

The detailed investigation on phase evolution during isothermal annealing can be understood with the help of Figure 3.4, 3.5 and 3.6. TEM investigation was carried out to investigate the fine microstructural features and it confirmed the phases present in LDHEA powder annealed at 700 ℃ (973K). The BF, SAD pattern, and DF images of annealed LDHEA powder were shown in Figure 3.7 (a), (b) and (c), respectively. The BF image of annealed powder shows that nearly cuboidal precipitates with a size of ~30-40 nm are

uniformly distributed in the powder particle. To confirm the structure of these annealed powder, SAD pattern was captured from the same powder particle being investigated. The polycrystalline rings corresponding to the parent BCC phase was confirmed from Figure 3.7 (b).

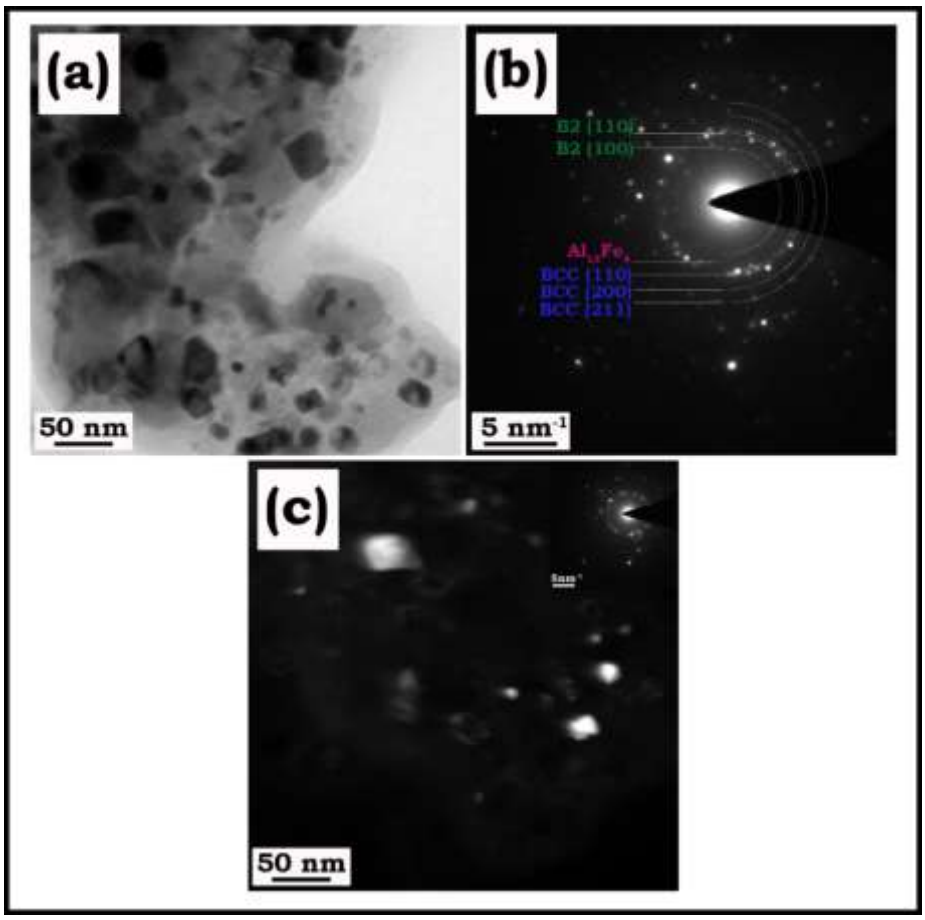

Figure 3.7: TEM micrograph showing (a) bright-field image; (b) corresponding SAD pattern; (c) dark-field image of MgAlSiCrFe HEA powder milled for 60 h follwed by annealing at 700 ℃ (973 K).

The rings corresponding to the (100) and (110) reflection of the B2-type AlFe phase and a weak intensity spot corresponding to the $Al_{13}Fe_4$ phase were observed. The presence of (100) ring of the B2 phase confirmed the formation of the ordered B2-type phase along with the parent BCC phase. The DF image shows the nanostructured nature of the cuboidal

precipitates and grains corresponding to the B2 and BCC phases respectively. The nanostructured grains of the BCC phase were estimated to have a size of ~25 nm even after isothermal annealing at 700 ℃ (973 K) for 1 h. This confirmed the thermal stability of nanostructured grains in LDHEA powder particles even after annealing.

3.2 Phase analysis and mechanical properties of the SPSed MgAlSiCrFe HEA

The detailed analysis of the phase evolution during mechanical alloying and the thermal stability of LDHEA powder particles provided an insight for consolidation of the milled powders through spark plasma sintering (SPS). The XRD pattern of the SPSed sample is shown in Figure 3.8. Figure 3.8 (a) shows that the parent BCC phase along with the B2-type AlFe, $Al_{13}Fe_4$, Cr_5Si_3 and β-Al_3Mg_2 phases were evolved. The peak position of these phases was marked in the enlarged peak pertaining to the (110) reflection of the BCC phase. During SPS, the parent BCC phase was found to retain its identity. In contrast to the isothermal annealing, the phase formed during SPS of mechanically alloyed powder was slightly different. The deconvoluted peak corresponding to the (110) reflection of the BCC phase shows three distinct peaks corresponding to (110) of B2-type AlFe and BCC phase along with a minor fraction corresponding to that of the $Al_{13}Fe_4$ phase (Figure 3.8 (c)). The change in the phase fraction of B2-type, BCC, and $Al_{13}Fe_4$ phases may be attributed to the non-equilibrium sintering mechanism involved during SPS. In case of isothermal annealing, the $Al_{13}Fe_4$ phase was the primary phase, followed by BCC and B2-type phases. However, the B2-type phase was the primary phase followed by BCC and $Al_{13}Fe_4$ phase, as discerned from the deconvoluted peaks shown in Figure 3.8 (c).

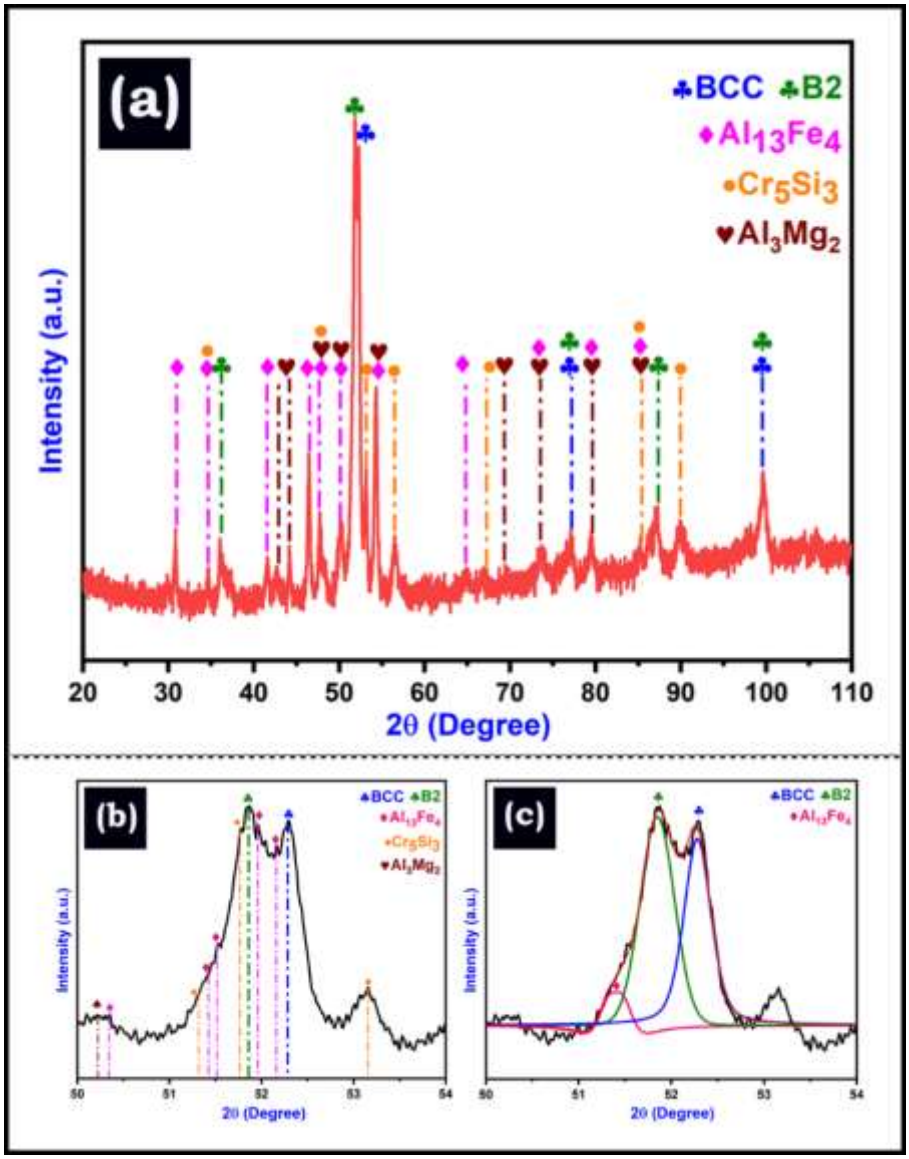

Figure 3.8: Phase evolution during spark plasma sintering of MgAlSiCrFe HEA at 800 °C (1073 K) (a); exploded image showing formation of minor phases along with the (110) peak of major phase (b); deconvolution showing the presence of minor $Al_{13}Fe_4$ phase with major BCC/ B2 phase (c).

The microstructural features of SPSed LDHEA can be understood with SEM micrographs shown in Figure 3.9 (a) and (b) at different magnification. it can also be observed that the particles having these three contrasts are uniformly distributed. The size of this light grey, dark grey, and dark contrast was found to be ~1.5-2.0 µm, ~1.0 µ, and ~0.5 µm respectively.

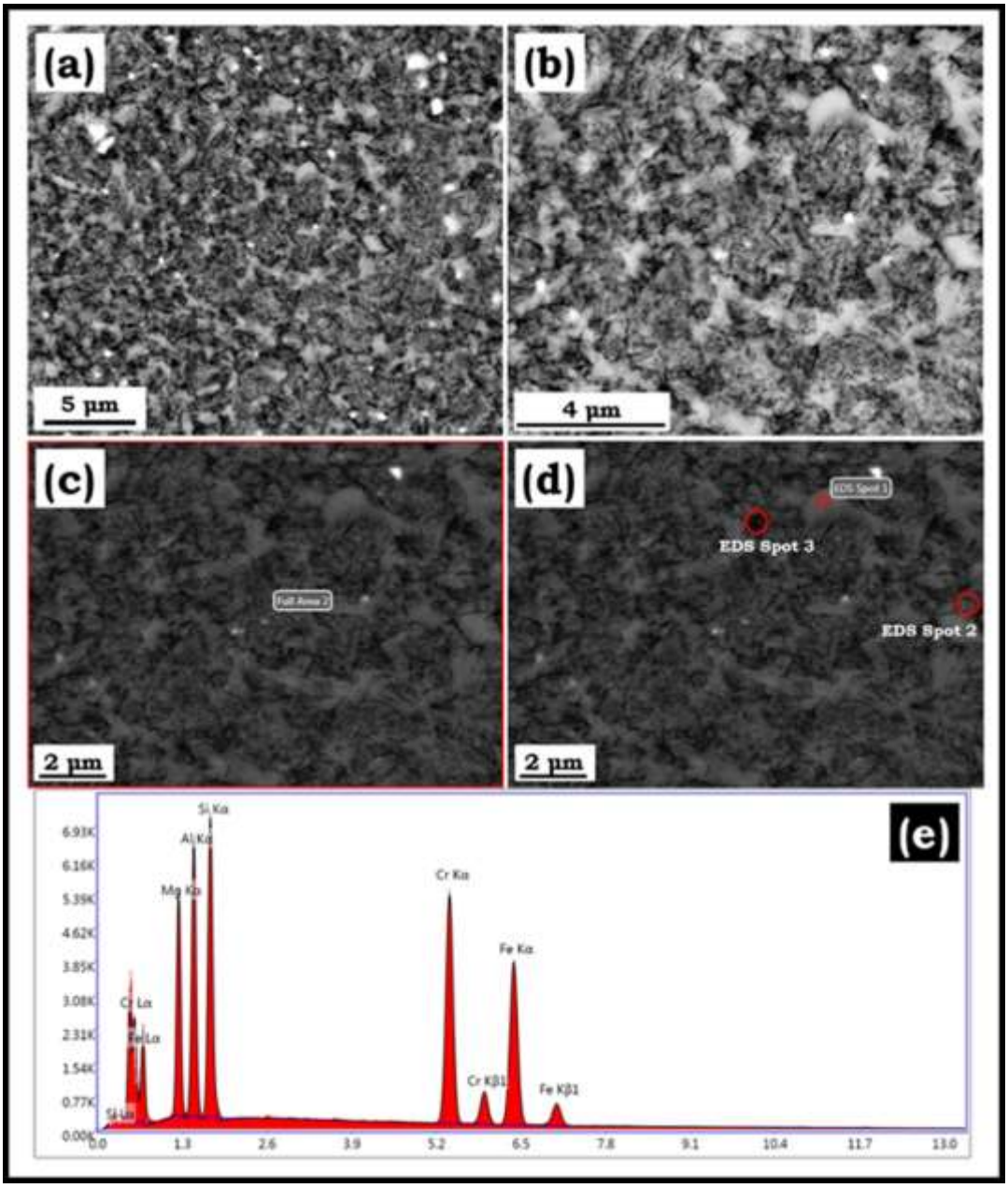

Figure 3.9: BSE-SEM micrograph showing the microstructure of MgAlSiCrFe HEA spark plasma sintered at 800 ℃ (1073 K). (a) microstructure at low magnification; (b) micostructure showing fine distribution of phases; (c) microstructure scanned for full area elemental mapping; (d) microstructure showing the spots for point SEM-EDS analysis; (e) EDS spectrum showing presence of alloying elements.

From the SEM micrograph, it can be discerned that the microstructure of SPSed sample has three distinctive contrasts, i.e., light grey, dark grey, and black contrast.

Furthermore, For ascertaining the chemical composition of these SPSed LDHEA, full area and point EDS analysis was conducted for the microstructure shown in Figure 3.9 (c) and (d) respectively. The EDS spectrum for the full area EDS scan is shown in Figure 3.9 (e). The nominal composition of the SPSed LDHEA sample is mentioned in Table I, which shows that the final composition after spark plasma sintering is almost the same as that of the milled LDHEA powder without significant variation. The nominal composition corresponding to the area of light grey contrast marked as EDS spot-1 was found to be rich in the Al and Fe.

Table 3.1: Elemental composition of spark plasma sintered MgAlSiCrFe HEA.

EDS Spot	Mg (at %)	Al (at %)	Si (at %)	Cr (at %)	Fe (at %)
Full Area	19.7	20.3	19.5	20.4	20.1
Spot 1	10.3	28.3	18.4	14.3	28.7
Spot 2	13.8	13.0	26.1	30.1	17.0
Spot 3	23.8	21.1	16.9	19.5	18.7

The phases with dark grey contrast marked as EDS spot-2 was rich in Cr and Si as mentioned in Table 3.1. Similarly, the phases having dark contrast marked as EDS spot-3 had an equiatomic elemental composition. Based on the EDS analysis, the light grey, dark grey and black contrast may correspond to the B2-type AlFe, BCC, and Cr_5Si_3 phases. These results are found to match with the findings of the XRD results. To understand further the elemental distribution of alloying elements in the LDHEA samples, SEM-EDS mapping was carried out (Figure 3.10). Figure 3.10 shows that almost all the elements were distributed homogenously as discerned from the intensity distribution of the alloying elements. However, at certain regions, the intensity corresponding to Al and Fe is observed

to be prominent. The Al and Fe rich region may be due to the presence of the B2-type AlFe phase. Based on the analysis of the XRD and SEM results for SPSed LDHEA, it can be stated that the B2-type AlFe is the primary phase, followed by the BCC phase.

The other intermetallics and silicide phases observed in the XRD pattern appear to be in minor amount, as evidenced from the SEM micrograph and the SEM-EDS mapping. The LDHEA sample prepared by SPS was almost dense ($\rho_{experimental}$=4.38 g.cm^{-3} with relative density of 99.98%) and had very appreciable microhardness, as mentioned in Table 3.2.

The MgAlSiCrFe SPSed sample's microhardness was ~7.11±0.31 GPa, and the estimated yield strength was found to be ~2.1GPa (Estimated YS=Hardness/3). Even at an indentation load of 500 g, no significant indentation cracks were observed for the MgAlSiCrFe SPSed LDHEA.

Table 3.2: Density and mechanical properties of SPSed MgAlSiCrFe HEA.

Sample	**Sintering Temperature (℃)**	**Density**		**Mechanical properties**	
		Experimental Density (g.cm^{-3})	**Relative density**	**Hardness (GPa)**	**Yield Strength (MPa)**
MgAlSiCrFe	800 ℃ (1073 K)	4.38	~99.98%	7.11 ± 31	2133

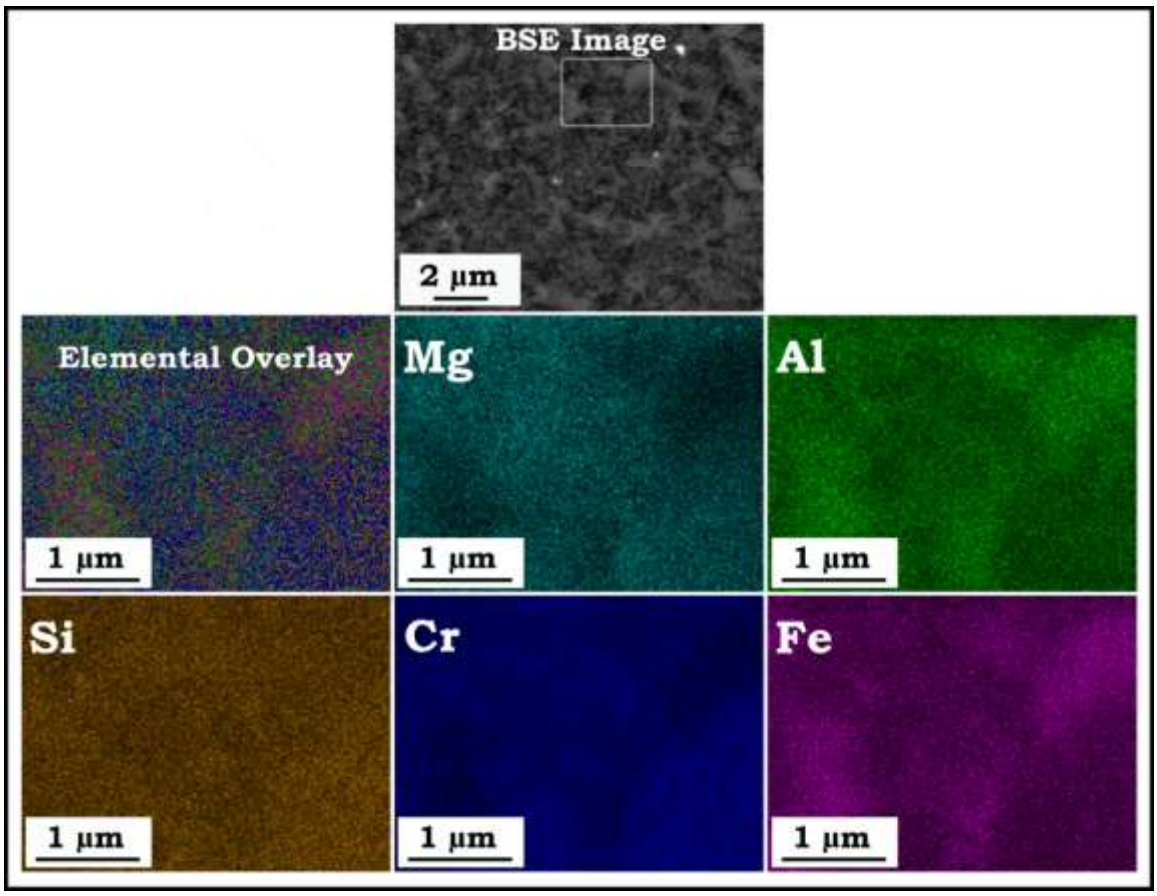

Figure 3.10: SEM-EDS mapping showing elemental distribution of MgAlSiCrFe HEA spark plasma sintered at 800 ℃ (1073 K).

From this, it may be inferred that the LDHEA fabricated by SPS has good indentation toughness. The structural and microstructural features and superior mechanical properties of these LDHEA can make them a candidate material for lightweight structural applications.

3.3. Discussion

The evolution of phases during mechanical alloying, isothermal annealing, and spark plasma sintering can be better understood using thermodynamic parameters and the CALPHAD approach through Thermo-Calc software. The preliminary investigation of the phase formation and stability are done using the Hume-Rothery rules-based parametric

approaches. The enthalpy of mixing (ΔH_{mix}^{ij}), atomic size mismatch (δ) factor, valence electron concentration (VEC), and few other parameters are calculated (**Table 3.3)**. Semi-empirical Miedema's model was used to calculate the enthalpy of mixing of the binary subsystems. The binary enthalpy values were extrapolated using a regular solution model to estimate the mixing enthalpy of the chosen quinary alloy.

Table 3.3: Physiochemical parameters and enthalpy of mixing of constituent elements in MgAlSiCrFe HEA.

Element	**Mg**	**Al**	**Si**	**Cr**	**Fe**
Atomic radius (Å)	1.62	1.438	1.18	1.249	1.241
Crystal structure	HCP	FCC	DC	BCC	BCC
Melting point (°C)	650	660	1410	1863	1538
Self-diffusion coefficient ($m^2.s^{-1}$)	10^{-13}	10^{-19}	10^{-62}	10^{-41}	10^{-31}
Electronegativity	1.2	1.6	1.9	1.6	1.8
Mg	**Mg**	-2	**-26**	24	18
Al		**Al**	-2	-10	-11
Si			**Si**	**-37**	**-35**
Cr				**Cr**	-1
Fe					**Fe**

According to Zhang et al. [131], the calculated parameters (enthalpy of mixing, VEC, and size mismatch) must fall within a specified range for the solid solution formation. The criteria for single-phase formation are as (i) $\Delta S_{config} \geq 13.38$ J.mol^{-1}K^{-1}, (ii) $-15 \leq \Delta H_{mix} \leq 5$ kJmol^{-1}K^{-1}, (iii) $\delta \leq 6.6\%$. Guo et al. [132] suggested additional criteria based on VEC to form a single-phase solid solution. According to this criterion, $VEC > 8$, $6.87 < VEC < 8$ and VEC < 6.87 can lead to FCC structure, a mixture of FCC and BCC structure, and BCC structure respectively.

Comparison of the results is presented in **Table 3.4**, which shows that the enthalpy of mixing (-15.84 kJ/mol) and the atomic size mismatch factor (~12) for MgAlSiCrFe is higher than the suggested limit. Thus, the possibility of the formation of a multiphase structure is a distinct possibility.

Table 3.4: Calculated thermodynamic and physical parameter of MgAlSiCrFe HEA.

	ΔH_{mix} $\left(kJ/mol\right)$	ΔS_{conf} $\left(\frac{JK^{-1}}{mol}\right)$	Tm (K)	Ω	δ (%)	VEC	Phase
Ideal	-15.0<ΔH_{mix}<7.0	≥13.38	-	≥1.1	<6.6	VEC≥8.0	FCC
						VEC<6.87	BCC
						6.87<VEC<8.0	BCC+FCC
Calculated	-15.84	13.38	1497	3.18	12	4.6	BCC

It is interesting to note that the Ω parameter (~3.12) favours the formation of a single-phase solid solution. However, due to more prominent role of enthalpy of mixing and atomic size mismatch factor on stability, the system eventually stabilizes into a multiphase structure. It is evident from the present investigation that the MgAlSiCrFe LDHEA crystallizes into a major BCC solid solution along with uniform distribution of reminiscent Si particles (~3 at%) as inferred from Figure 3.1, 3.2, and 3.3. Therefore, apart from the thermodynamic parameters discussed until now, a few other factors (i.e. atomic radii, crystal structure, melting point, self-diffusion co-efficient etc.) also influence the phase evolution during mechanical milling as illustrated in **Table 3.3**. It is usually believed that the dissolution of alloying element and phase evolution during milling depends on its melting point. Having a higher bond strength, it usually acts as a host lattice of other

alloying elements in multicomponent alloys. In the present investigation, the major BCC solid solution phase has lattice parameter ~0.2887±0.005 nm, which is very close to the lattice parameter of α-Fe. Similar findings were reported by Shivam et al. [133–135] during the systematic investigation of phase evolution during MA of AlCoCrFeMnNi, AlCoCrFeNi and AlCoCrFeNiTi HEAs. They have explained the influence of the melting temperature of alloying elements on the preferential affinity to form a host lattice. The dissolution of elements mainly depends upon the bond strength. Contrary to this, in the present investigation the Si (~3 at%) was retained in the LDHEA. This anomaly in the phase evolution during milling of MgAlSiCrFe LDHEA powder can be explained with other physical parameters like self-diffusion co-efficient as reported in **Table 3.3**. However, this aspect of alloying of Si in the HEAs requires further investigations. The influence of the self-diffusion parameter on the phase formation in LDHEA was demonstrated by Pandey et al. [136]. They have observed that the elements like Mn and Si having low self-diffusion coefficient are not fully dissolved in the solid solution. A minor fraction of these elements can retain their identity even after prolonged milling. In case of the MgAlSiCrFe LDHEA, the self-diffusion coefficient (*D*) follows the sequence: $D(\text{Si}) < D(\text{Fe}) < D(\text{Cr}) < D(\text{Al}) < D(\text{Mg})$ as mentioned in **Table 3.3**. Although the melting temperature of Si is less than that of Fe and Cr, however, a minor fraction of Si remains undissolved even after 60 h of milling due to its lower self-diffusion coefficient as well as non-metallic nature of Si atoms among other factors. Aravindh et al. [137] systematically performed theoretical calculations using DFT for understanding the effect of incorporating Si into CoCrFeNi HEA on its structural, electronic, and mechanical properties. They found that incorporating Si up to 12.5% did not change the non-covalent nature of the interaction between Si and other alloying elements in the CoCrFeNiSix (x=12.5%) HEA. However, a

change in the nature of interaction from non-covalent to covalent was observed by them in CoCrFeNiSi HEA having a Si content of more than 12.5%. The DFT calculation done by Aravindh et al. [137] confirmed the exciting electronic and magnetic properties of these HEA without having any detrimental effect on mechanical properties.

The binary enthalpy values estimated using Miedema's model could act as a critical parameter to understand the type of binary interactions between the constituent elements in a multi-component alloy (**Table 3.3)**. The evolution of phases during mechanical alloying and isothermal annealing can also be inferred with the help of the CALPHAD approach through Thermo-Calc software, as evident from the binary phase diagrams (for the sub-systems) and the property diagram for the MgAlSiCrFe HEA, shown in Figure 3.11 (a-g) and Figure 3.12 respectively. The binary phase diagrams of all the binary subsystems of MgAlSiCrFe LDHEA was calculated and displayed in figure 3.11. Analysing these phase diagrams, it can be seen that none of the elemental pair shows an isomorphous mixing. The binary systems Mg-Cr and Mg-Fe showed very high liquid phase miscibility gaps, whereas the Cr-Fe system has solid-state miscibility. The other binary systems, such as Mg-Al, Mg-Si, Al-Cr, Al-Fe, Cr-Si, and Fe-Si, show multiple intermetallic phases stable at room and high temperatures. From this assessment, it is clear that there is a clear tendency to form intermetallic phases. The remaining three binary systems have a small negative deviation from the ideal condition, indicating possibility of less clustering. From the analysis of the phase diagrams, we can predict that there is a likelihood of different elements resulting in forming a large number of intermetallic phases. This prediction is also supported by the large variation of electronegativity value among the constituent elements (**Table 3.3**). Furthermore, the phase transformation occurring during the isothermal annealing and SPS can be inferred through a property diagram showing the variation of the phases as a function

of temperature generated by CALPHAD modeling (Figure 3.12). From Figure 3.12**,** it is obvious that there is a mixture of two liquids (representing liquid phase miscibility gap). The first phase, Cr_5Si_3, precipitated from the Liquid#2 at approximately 1270 °C.

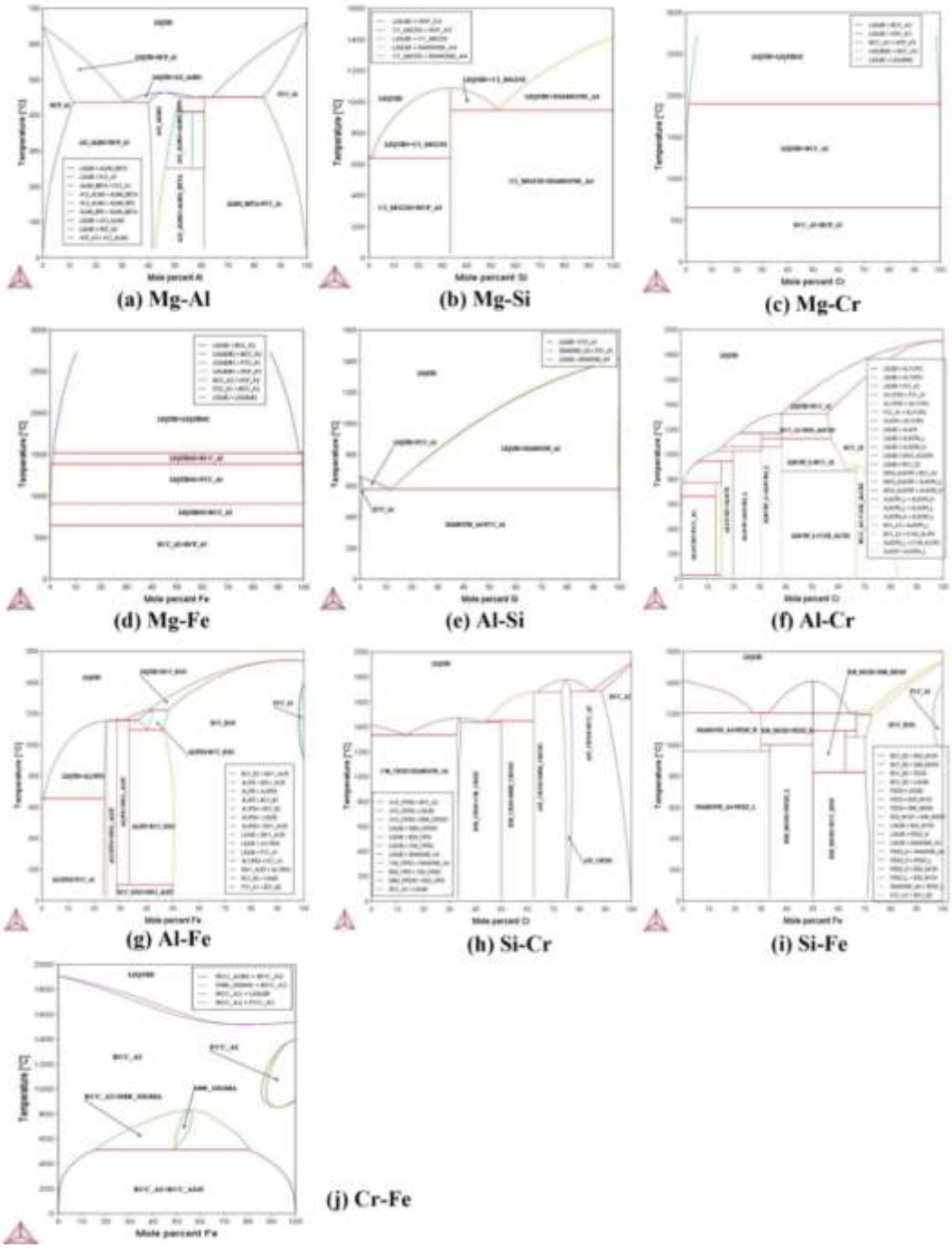

Figure 3.11. Binary phase diagrams (binary subsystems of MgAlSiCrFe HEA) calculated by Thermo-Calc (SSOL5 database)

The second phase, BCC_B2, also precipitated from the LIQUID#2 at ~1100 °C. The number of phases remained unaltered before ~880 °C, at this point, and the third phase Mg_2Si precipitated from the second liquid phase (Liquid). All the liquid solidified to Mg_2Si at ~725 °C, and the fraction of Cr and Si elements diffused from the Cr_5Si_3 to form Cr_3Si. A small amount of Al_2Fe precipitated from the BCC_B2 phase at ~800 °C. The single point equilibrium calculation for the MgAlSiCrFe high entropy alloy is tabulated in **Table 3.4**. The table presents the phase fraction and the composition of phases at various temperatures. At 1400 °C, a mixture of two liquids is stable, showing the Mg-rich liquid phase (Liquid) and approximately equiatomic liquid phase of Al, Si, Cr, and Fe elements (Liquid#2). From the compositional analysis of the phases at 1000 °C, it was inferred that the BCC_B2 phase would be Al-Fe rich.

The binary phase diagram showed that an ordered Cr_5Si_3 phase being a congruent phase obtained from Cr and Si-rich liquid phase as reported by Gokhale et al. [138], precipitated out first as shown in figure 3.12.

Table 3.5: Single point equilibrium calculation is done to estimate phase fraction and phase composition as a function of temperature.

Temp.	Phases	Phase Frac.	Mg	Al	Si	Cr	Fe
1400 (°C)	Liquid	0.433	0.598	0.194	0.194	0.005	0.008
	Liquid#2	0.566	0.024	0.285	0.267	0.221	0.203
1000 (°C)	Liquid	0.281	0.709	0.165	0.123	0	0.002
	BCC_B2	0.433	0.001	0.355	0.134	0.060	0.499
	CR5SI3	0.286	0	0	0.375	0.607	0.017
	BCC_B2	0.354	0	0.444	0.050	0.008	0.497

600 (°C)	MG2SI	0.300	0.667	0	0.333	0	0
	CR3SI_A15	0.186	0	0	0.250	0.738	0.011
	CR5SI3	0.095	0	0	0.375	0.623	0.002
	AL2FE	0.064	0	0.667	0	0	0.333
300 (°C)	BCC_B2	0.372	0	0.471	0.025	0	0.504
	MG2SI	0.300	0.667	0	0.333	0	0
	CR3SI_A15	0.146	0	0	0.250	0.748	0.002
	CR5SI3	0.144	0	0	0.375	0.625	0
	AL2FE	0.037	0	0.667	0	0	0.333

Similarly, the BCC_B2 phase rich in Al and Fe, having high-temperature stability, led to precipitation of the second phase from liquid. The third phase precipitated as Mg_2Si at approximately 800 °C from the remaining liquid phase being rich in Mg and Si. The precipitation of various phases along with the transformation temperature, as shown in Figure 3.12 can be summarized below:

Phase transformation	**Temperature**
Liquid#2 → Cr_5Si_3	1270 °C
Liquid#2 → BCC_B2	1100 °C
Liquid → Mg_2Si	880 °C
BCC_B2 → Al_2Fe	790 °C
Cr_5Si_3 → Cr_3Si	730 °C

Considering Figure 3.12 and Table 3.3**,** it can be estimated that the major phase BCC_B2 with phase fraction of 0.372) was the Al and Fe rich phase with a small amount

of Si. The second major phase at 300 °C was Mg_2Si with phase frac. 0.3), followed by Cr_3Si of phase frac. 0.146), Cr_5Si_3 (phase frac. 0.144), and Al_2Fe (Phase frac. 0.037). Thus all the phases obtained at room temperature were ordered phases. The phases predicted through the Thermo-Calc software are in somewhat close approximation with the phases observed during isothermal annealing and spark plasma sintering of mechanically alloyed LDHEA powders. During the isothermal annealing, the B2-type AlFe phase and Mg_2Si phase was observed along with the parent BCC phase (Figure 3.5). Further increasing the annealing temperature led to the preferential formation of the Cr_5Si_3 phase at the expense of the Mg_2Si phase. Furthermore, the SPS of LDHEA powder at 800 ℃ enhanced the phase fraction of the B2-type AlFe phase compared to the parent BCC phase, other intermetallics, and silicides, as evident from Figure 3.12. The anomaly in the phase prediction through Thermo-Calc and experimental findings may be attributed to the limitation of the SOSL5 database instead of the TCHEA database for CALPHAD modeling.

The MgAlSiCrFe SPSed LDHEA samples were found to have an excellent hardness ~7.11±0.31 GPa and an estimated yield strength of ~2.1 GPa. This LDHEA was found to have a low-density of ~4.38 $g.cm^{-3}$ with a relative density of 99.98%. The high hardness and strength of these LDHEA may be attributed to the B2-type AlFe and BCC phases along with intermetallics particles like $Al_{13}Fe_4$, β-Al_3Mg_2, Cr_5Si_3, and FCC2 solid solution. A few researchers and co-workers have attributed superior mechanical properties due to the formation of intermetallics like $CuMg_2$, $MgCu_2$, σ- phase corresponding to Fe-Cr, ordered AlFe type phases [62,139].

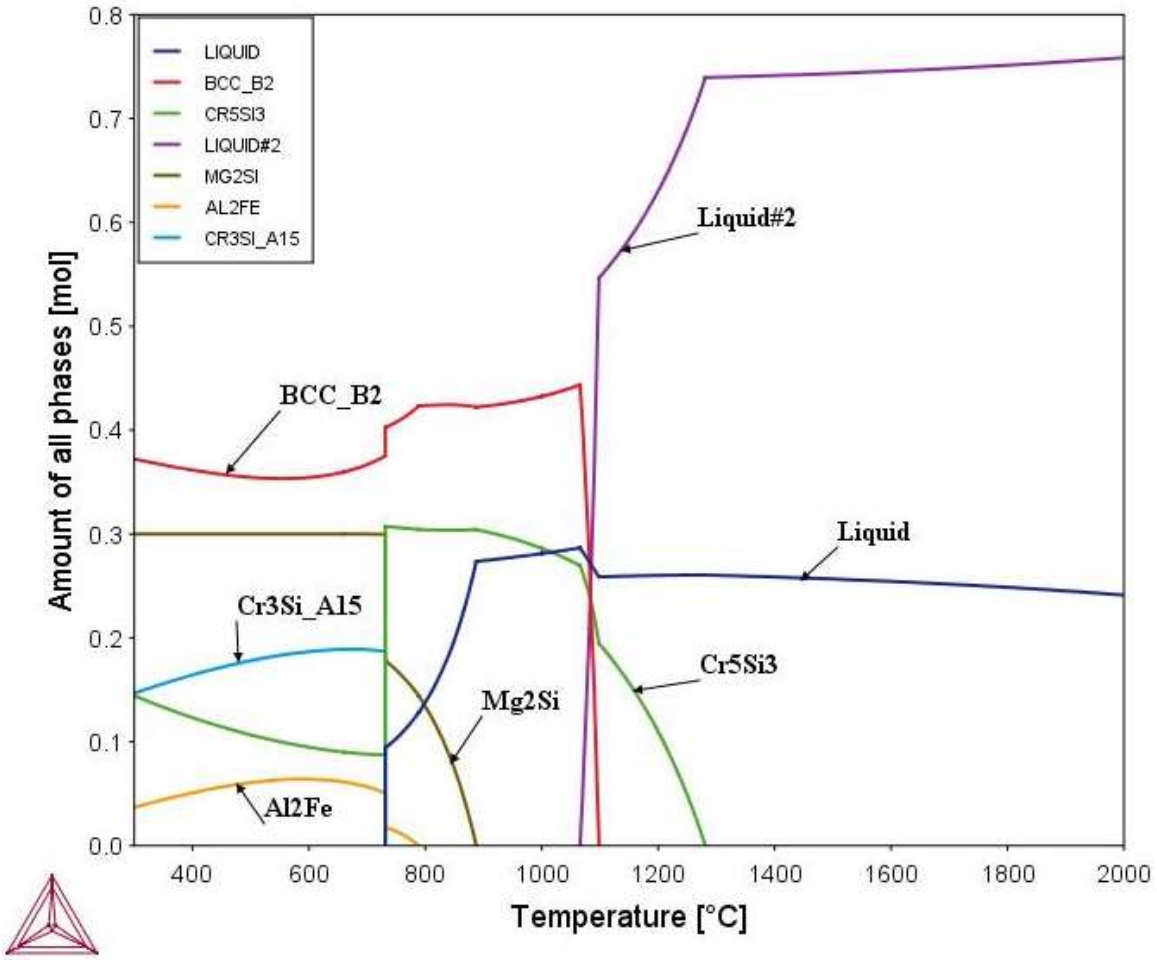

Figure 3.12: Property diagram of MgAlSiCrFe HEA using Thermo-Calc (SSOL5 database).

Increasing the fraction of Mg content in the $AlFeCuCrMg_x$ (x=0,0.5, 1.0, 1.7) HEA leads to the enhancement of hardness and strength due to an increase in the amount of ordered B2-type AlFe. Chae et al. [140] have fabricated an equiatomic AlCuFeMnMgTi low-density HEA with a density of 4.34 $g.cm^{-3}$ through ball milling and SPS. They have observed the formation of two types of BCC phases (i.e., BCC1 and BCC2 lean and rich in Mg, respectively) along with a minor fraction belonging to Cu_2Mg and retained Ti. The elemental Ti was not fully incorporated into the solid solution even after 60 h of mechanical alloying due to its higher melting point and HCP crystal structure. They further noticed

that on sintering these LDHEA powder through SPS, the phase fraction of the BCC2 phase increases considerably along with the Cu_2Mg intermetallics, which indeed resulted in a bulk LDHEA having a high hardness of ~770 HV. In yet another development, Chauhan et al. [92] attempted to develop $Al_{35}Cr_{14}Mg_6Ti_{35}V_{10}$ (at%) LDHEA by 30 h of mechanical alloying followed by SPS at 750 ℃. After MA, a single-phase BCC solid solution was formed, transforming into two BCC phases and one HCP phase after SPS. Although they achieved a low-density HEA having a 4.05 g.cm-3 after SPS, due to low-temperature sintering, the relative density was ~85%. However, in this present work, SPS was done at 800 ℃ to fabricate a bulk LDHEA compact with an experimental density almost comparable to that of the theoretical density. A work conducted by Mishra and Sahi [141] has shown the formation of a BCC and FCC phase for an equiatomic AlFeMgNiTi LDHEA. On isothermal annealing of these mechanically alloyed LDHEA powder, they observed the preferential increase in the BCC phase fraction in these LDHEAs. The literature suggests the formation of multiphase LDHEA containing low-density elements like Mg. Apart from Mg, alloying elements like Si also influence HEAs phase evolution and mechanical properties. A few researchers and co-workers have shown the effect of Si addition on the phase formation, thermal stability, and mechanical properties of HEA. In a recent study, Sharma et al. [101] have shown the effect of sintering temperature on the densification behavior, phase formation, and mechanical properties of AlCuSiZnFe light-weight HEA. They have reported a major FCC phase with a minor fraction corresponding to the BCC solid solution after 45 h of mechanical alloying. They have also observed that even after MA for 45 h, some reminiscent Si was present. They have observed phase transformation during SPS at 600 ℃ to 800 ℃. On increasing the SPS temperature, the phase fraction of the BCC phase considerably increases, and at 800 ℃ this leads to the formation of

intermetallic compounds. The SPS at 650 ℃ and 700 ℃ led to the formation of the minor amount of Fe-Si rich and Al-Fe-Si rich particles, respectively, due to the dissolution of retained Si at these temperatures. These intermetallics and the FCC as well as BCC phases at 650 ℃ were responsible for the high compressive strength (~1900 MPa) with appreciable failure strain (~19%). The high hardness and estimated yield strength of MgAlSiCrFe LDHEA fabricated through SPS may also be attributed to silicides like Mg_2Si and Cr_5Si_3 along with other intermetallics and BCC parent phase. Recently, Hasan et al. [142] have attempted to synthesize $Al_{24.2}Si_{3.2}Cu_{24.2}Ti_{24.2}Ni_{24.2}$ (at%) low-density HEA by physical blending through probe sonication followed by conventional sintering. They have found the presence of high entropy intermetallics particles after pressureless sintering at 600 ℃ (873 K). These intermetallics particles formation was indeed responsible for enhanced microhardness and compressive strength of ~1100 MPa and ~310 MPa, respectively with an appreciable failure strain of ~14%. Cheng et al. [143] have shown the effect of Si in Al0.3CoCrFeNiSix (x=0, 0.2, 0.5, 0.8, 1.0) HEA and have established its impact on the phase evolution and mechanical properties. They have observed the formation of HEA with Si (x=0.0) has an FCC solid solution. However, increasing the fraction of Si from x=0.2 to x=1.0, the phase fraction of the BCC/B2-type phase increases and is almost more than 90% for x=1.0. They have also shown the co-existence of BCC and B2-type Al, Ni, Si-rich phases by deconvolution of XRD peak corresponding to the (110) reflection of BCC phase. The increase in Si from x=0 to 1.0 considerably increases its hardness from 143 HV to 826 HV. They have discerned that the drastic enhancement in the hardness and strength of these HEA can be attributed to the phase transformation of FCC to BCC/ B2-type phases and homogenous precipitation of BCC phase in the B2-type grains. The equiatomic fraction of Si in MgAlSiCrFe LDHEA enhances the formation of a major B2-type AlFe

phase in addition to the parent BCC phase. The non-equilibrium sintering mechanism being encountered during SPS of these LDHEA may be responsible for the preferential enhancement of B2-type AlFe phase in comparison to other phases observed in case of isothermal annealing. The present understanding of the phase evolution during MA, isothermal annealing, and SPS will be of importance and interest for fabricating LDHEAs with a single-phase solid solution along with the desired phases and its consequent effect on mechanical properties.

3.4. Conclusions

The following conclusions can be made from the present chapter:

1. Enthalpy of mixing of the MgAlSiCrFe alloy calculated using Miedema's model (ΔH_{mix} ~ -15.84 kJ/mol) and atomic size mismatch factor (12 %) lies outside the solid solution formation range ($-15 \leq \Delta H_{mix} \leq 5$ kJmol^{-1}K^{-1}, $\delta \leq 6.6\%$) indicating the possibility of multiphase structure. Hence the experimental observation of two phases in the mechanically alloyed LDHEA (i.e., a major BCC phase with ~3% of retained Si) agrees with the parametric calculations. However, the annealed and SPSed samples showed multiphase structures not following the criteria for the formation of a single solid solution phase.
2. As per the prediction of the CALPHAD approach, five ordered phases are stable at 300 °C (573 K). The major phase being Al and Fe rich B2 phase (0.372) and Mg_2Si (0.300). However, three binary, ordered intermetallic phases (Cr_5Si_3, Cr_3Si, and Al_2Fe) are also present in minor amounts.
3. Experimental observation during isothermal annealing confirmed the formation of ordered B2-type AlFe, along with parent BCC phase, intermetallics, and silicides.

The minor fraction of other intermetallics and silicides at a higher temperature may be attributed to the sluggish diffusion effect. Further, the cuboidal B2-type AlFe precipitate was found to be homogeneously distributed in the BCC powder particles annealed at 700 ℃ (973K).

4. The phases formed during SPS of MgAlSiCrFe LDHEA mechanically alloyed powders were slightly different from those of annealed powders. It contained a major B2-type AlFe and BCC phases along with a minor amount of $Al_{13}Fe_4$, β-Al_3Mg_2 intermetallic phase and Cr_5Si_3 silicide phases. The non-equilibrium sintering mechanism during SPS might have led to the transformation of FCC2 ($Al_{2.4}Mg_{1.6}$) solid solution into β-Al_3Mg_2 intermetallic phase.
5. The SPSed sample had exhibited a low-density of ~4.38 $g.cm^{-3}$ with a relative density of ~99.98%. The formation of the B2-type AlFe phase and the BCC phase and minor amounts of intermetallics and silicide may be responsible for the high hardness ~7.11±0.31 GPa of these SPSed MgAlSiCrFe LDHEA without any signature of indentation cracks.